Journal of Digital Imaging (2019) 32:175–182
https://doi.org/10.1007/s10278-018-0119-2

Automatic Mapping of CT Scan Locations on Computational Human Phantoms for Organ Dose Estimation

Choonsik Lee[1,2] · Gleb A. Kuzmin[1] · Jinyong Bae[3] · Jianhua Yao[4] · Elizabeth Mosher[1] · Les R. Folio[4]

Published online: 5 September 2018

Abstract
To develop an algorithm to automatically map CT scan locations of patients onto computational human phantoms to provide with patient-specific organ doses. We developed an algorithm that compares a two-dimensional skeletal mask generated from patient CTs with that of a whole body computational human phantom. The algorithm selected the scan locations showing the highest Dice Similarity Coefficient (DSC) calculated between the skeletal masks of a patient and a phantom. To test the performance of the algorithm, we randomly selected five sets of neck, chest, and abdominal CT images from the National Institutes of Health Clinical Center. We first automatically mapped scan locations of the CT images on a computational human phantom using our algorithm. We had several radiologists to manually map the same CT images on the phantom and compared the results with the automated mapping. Finally, organ doses for automated and manual mapping locations were calculated by an in-house CT dose calculator and compared to each other. The visual comparison showed excellent agreement between manual and automatic mapping locations for neck, chest, and abdomen-pelvis CTs. The difference in mapping locations averaged over the start and end in the five patients was less than 1 cm for all neck, chest, and AP scans: 0.9, 0.7, and 0.9 cm for neck, chest, and AP scans, respectively. Five cases out of ten in the neck scans show zero difference between the average manual and automatic mappings. Average of absolute dose differences between manual and automatic mappings was 2.3, 2.7, and 4.0% for neck, chest, and AP scans, respectively. The automatic mapping algorithm provided accurate scan locations and organ doses compared to manual mapping. The algorithm will be useful in cases requiring patient-specific organ dose for a large number of patients such as patient dose monitoring, clinical trials, and epidemiologic studies.

Keywords Computed tomograpy · Dosimetry · Scan location · Computational human phantoms

Introduction

The use of CT examinations has increased dramatically over the past few decades [1, 2]. This increase reflects a rapid surge in exposures from all medical sources, which made up 15% of the per capita effective dose in 1982 and 48% in 2006 [3]. About half of the per capita effective dose from medical exposures in 2006 was due to CT examinations. In order to make informed decisions in practicing CT, a better understanding of the nature and magnitude of radiation dose and health risk resulting from CT examinations is crucial. National and other standards [4] require modern CT scanners provide simplified and measurable dose descriptors such as CT dose index (CTDI) and dose length product (DLP) as a surrogate of dose delivered to a patient. Another dose descriptor more relevant to patient dose, called effective dose, can be derived from DLP using pre-calculated conversion factors [5]. Size-specific dose equivalent (SSDE), a volumetric CTDI ($CTDI_{vol}$) weighted by body size, is also recommended by the American Association of Physicists in Medicine (AAPM) [6]. However, these dose descriptors are fundamentally based on the two cylindrical CTDI phantoms with the diameter of 16 and 32 cm. In epidemiologic or clinical researches of computed tomography (CT) patients, radiation dose to organ or tissue

✉ Choonsik Lee
choonsik.lee@nih.gov

[1] Division of Cancer Epidemiology and Genetics, National Cancer Institute, National Institutes of Health, Bethesda, MD, USA

[2] Radiation Epidemiology Branch/DCEG/NCI/NIH, 9609 Medical Center Drive, Rockville, MD 20850, USA

[3] Kansas City University of Medicine and Bioscience, Kansas City, KS, USA

[4] Radiology and Imaging Sciences Clinical Center, National Institutes of Health, Bethesda, MD, USA

of a patient is often sought to evaluate potential relationship with the risk of adverse health effect [7, 8].

Organ dose estimates can be obtained through measurements combined with physical anthropomorphic phantoms or computer simulations of CT X-ray and computational models of human anatomy. Once validated by measurements, simulation approach is flexible and cost-effective. Based on the organ dose database derived from simulations, several dose calculation tools [9–14] are available for CT patients. One of the key components in the dosimetry tools is a computational human phantom, essentially a computer model of human anatomy. Various types of computational human phantoms ranging from the early stylistic models [15] to anatomically realistic ones based on radiological images of patients [16] have been adopted in different CT dosimetry tools. Some recent dose calculation tools automatically extract technical scan parameters from the header of DICOM files to facilitate more accurate and automated organ dose calculations. Among the scan parameters affecting organ doses, scan locations are critical especially for organs partially covered by scan range or close to scan boundaries [17–19]. However, it is challenging to accurately map the patient's scan locations on the anatomy of computational human phantoms because there is no coordinate information provided from CT scanners.

Different approaches have been used to map patient's CT scan location on computational human phantoms. First, one can assume that standard scan protocols are consistently used for patients across the whole cohort. For example, a general chest CT protocol starting from the top of the clavicles and ending at the middle of the liver can be assumed to be used for all chest CT patients. This approach is often used in studies where CT images are not readily available or there are too many CT images to retrieve [20–22]. However, significant dosimetric uncertainty cannot be avoided especially for organs partially included in the scan range. Second, in cases where scan-specific $CTDI_{vol}$ and DLP are available from DICOM data, scan length can be derived through dividing DLP (mGy-cm) by $CTDI_{vol}$ (mGy). Scan length then can be added to protocol-based scan start to decide scan end location [23, 24]. However, it is still uncertain how the given scan length is distributed across the patient anatomy. Finally, mapping can be manually conducted by experienced radiologists if the number of patients involved is relatively small, which is not practical for a large number of scans. At present, no automated and reliable methods to map patient scan locations on computational human phantoms are available.

We introduce an algorithm to automatically map the CT scan locations of patients on computational human phantoms. The algorithm compares two skeletal masks obtained from a patient and a computational human phantom to decide the best matching scan locations. To test the performance of the algorithm, we randomly selected five sets of neck, chest, and abdominal CT images from the National Institutes of Health Clinical Center and automatically mapped the scan locations from those CT images on a computational human phantom using our algorithm. We then compared the automated mapping with those manually mapped by radiologists. Finally, organ doses for automated and manual mapping locations were calculated by an in-house CT dose calculator and compared to each other.

Materials and Methods

CT Images

We obtained five sets of anonymized CT images for neck, chest, and abdomen-pelvis (AP) exams totaling 15 image sets from the National Institutes of Health Clinical Center, under an Internal Review Board (IRB)-exempt study protocol. Neck CT exams were on adult males with an average age of 59 (48–65 years). Chest and abdomen and pelvis (AP) scans were obtained from adult male patients with an average age of 52 years (45–58 years), who were different from the neck CT patients. To facilitate the analysis, the five neck scans were randomly grouped to the five chest and AP CT scan sets and named patient 1 to 5.

CT-to-Phantom Mapping Algorithm

To map the scanning location of the patient CTs on the computational human phantoms, we adopted an algorithm we previously developed to extend partial body CT images to whole body [25]. The algorithm generated a two-dimensional (2D) skeletal mask by using ray-tracing from the front to back of a patient from a given patient CT set by applying a threshold of Hounsfield unit (285–3500) to CT pixels. Then, the patient CT-based skeletal mask was compared with the pre-generated whole body skeletal mask of the adult male computational phantom [26]. The pre-generated phantom skeletal mask was linearly scaled in the lateral and antero-posterior direction to match the outer contour dimensions of the patient measured on the first and last image slices of the patient CT. As shown in Fig. 1, we scanned the whole-body phantom mask (Fig. 1b) with the patient skeletal mask (Fig. 1a) from the top of the head to the bottom of the feet of the phantom with the vertical increment of 0.5 cm. For each increment, a Dice Similarity Coefficient (DSC) was calculated between the patient and phantom skeletal masks as follows:

$$DSC(z) = \frac{2N(Ph(z) \cap Pa)}{N(Ph(z)) + N(Pa)} \quad (1)$$

where N is an operator providing the number of pixels of value 1 in a binary skeletal mask, Pa is the 2D skeletal mask of the patient derived from the patient's CT, and $Ph(z)$ is the 2D

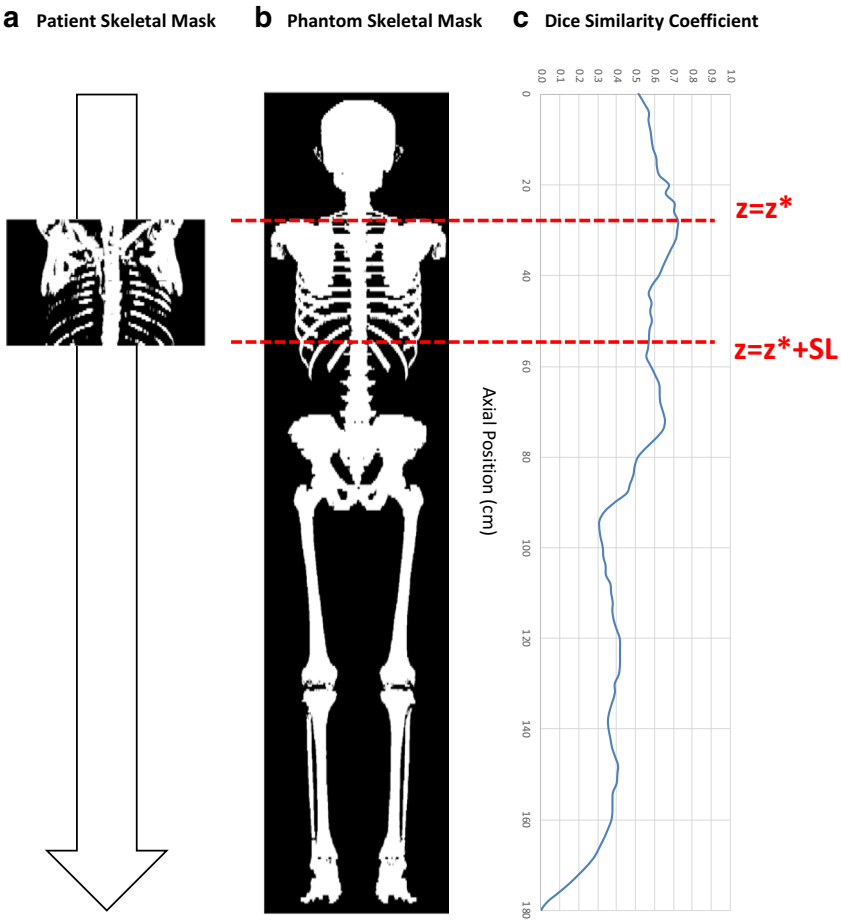

Fig. 1 Workflow of the automatic mapping algorithm: **a** The patient-specific skeleton mask was compared with **b** the pre-generated skeleton mask of the whole body phantom by calculating **c** DSC at each vertical increment of 0.5 cm

skeletal mask of the whole-body computational phantom cropped to match the length of the patient CT at the level z *cm* from the top of the head. The *DSC* can range from 0 to 1, where a value of 0 represents the case the patient and phantom skeletal masks do not match at all and a value of 1 represents the case where the masks match completely. The *DSC* will reach a maximum at some optimal index coordinate z^* *cm* (Fig. 1c). The optimal z-position, z^*, is selected as the scan start location and the scan end location was calculated by adding the scan length (SL) to the optimal scan start, z^*. The mapping algorithm was written in Python computer language with text-based user interface to automatically import and process CT images.

Manual Mapping by Radiologists

To test the performance of the automatic mapping algorithm, we asked seven radiologists to manually map the neck, chest, and AP CTs of the patient 1 to 5 on the computational human phantom. First, we generated sagittal images from the neck CTs and coronal images from the chest and AP CTs. We showed the cross-sectional images to each radiologist independently for them to manually mark the location of the scan start and end of the patients on an adult male computational phantom. The manual mapping was conducted blind to the results from other radiologists and from the automatic mapping algorithm. Each radiologist provided the scan start and end locations mapped on the computational phantom for the five neck, five chest, and five AP CT sets. We then compared the manual scan locations with those obtained from the automatic algorithm.

Organ Dose Calculations

To investigate the dosimetric accuracy of the automatic mapping algorithm, we also compared key organ doses calculated for both sets of scan locations. We adopted an in-house organ dose calculator, National Cancer Institute dosimetry system for CT (NCICT) [10], for organ dose calculations. A comprehensive set of organ dose conversion coefficients, which convert $CTDI_{vol}$ to organ dose, is built in NCICT, which was computed from Monte Carlo radiation transport technique combined with a series of reference size pediatric and adult computational human phantoms. The graphical user interface of the program was also used to facilitate the manual mapping process by the radiologists. Since we did not need an absolute organ dose for the purpose of this study, we assumed $CTDI_{vol}$ of unity, the tube potential of 120 kVp, and the body filter for

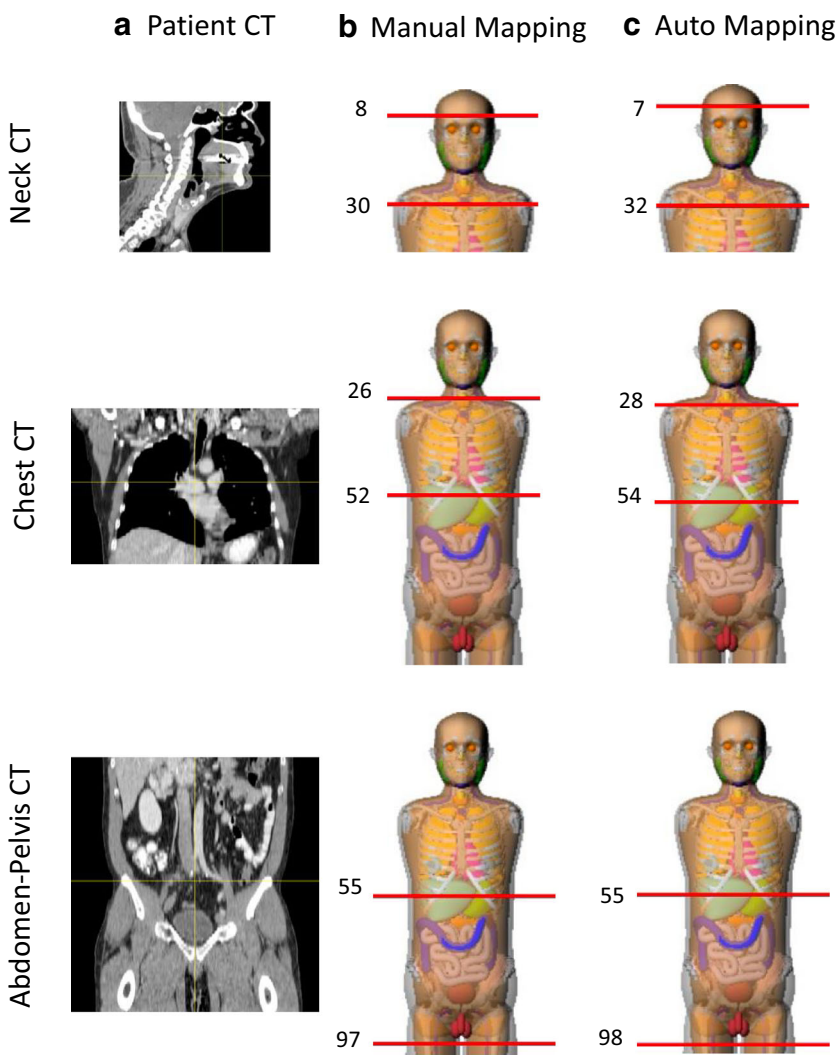

Fig. 2 **a** The cross-sectional images for neck, chest, and AP CTs of patient 1. The scan start and end locations for patient 1 **b** manually mapped by radiologists and **c** automatically mapped by the algorithm

the neck, chest, and abdominal scans. First, we calculated $CTDI_{vol}$-normalized organ dose (mGy/mGy) for the five neck, chest, and AP CTs using the scan locations automatically mapped by the algorithm. Then, we calculated organ dose for the manual mapping data using the averaged scan locations of the seven radiologists.

Results

Automatic Mapping Algorithm

Figure 1 shows an example of the automatic mapping for the chest CT of patient 1. The patient-specific skeleton mask (Fig. 1a) was compared with the pre-generated skeleton mask of the whole body phantom (Fig. 1b) by calculating DSC at each vertical increment of 0.5 cm from the top of the head (0 cm) to the bottom of the feet (180 cm) of the whole body phantom (Fig. 1c). The maximum DSC of 0.73 was obtained at $z = 28$ cm, which was mapped as scan start location, and $z = 54$ cm was mapped as scan end location by adding the scan length of 26 cm to the scan start, $z = 28$ cm. The next highest DSC of 0.66 was obtained at $z = 72$ cm around the pelvis region. The scan start and end locations were decided by using the same process for the neck, chest, and AP CTs of patient 1 to 5. The automatic mapping process took about one to a minute for each CT depending on the size of skeletal masks.

Comparison of Scan Locations with Manual Mapping

Manual mapping was conducted by the seven radiologists and used as the ground truth in the comparison with the results from automatic mapping. The manual mapping was conducted by using the cross-sectional image sets for neck, chest, AP CTs, and NCICT program. It took about 15 min for a radiologist to finish mapping all 15 sets of CTs on the computational phantom. Figure 2a shows the cross-sectional images for neck, chest, and AP CTs of patient 1 that were sent to the

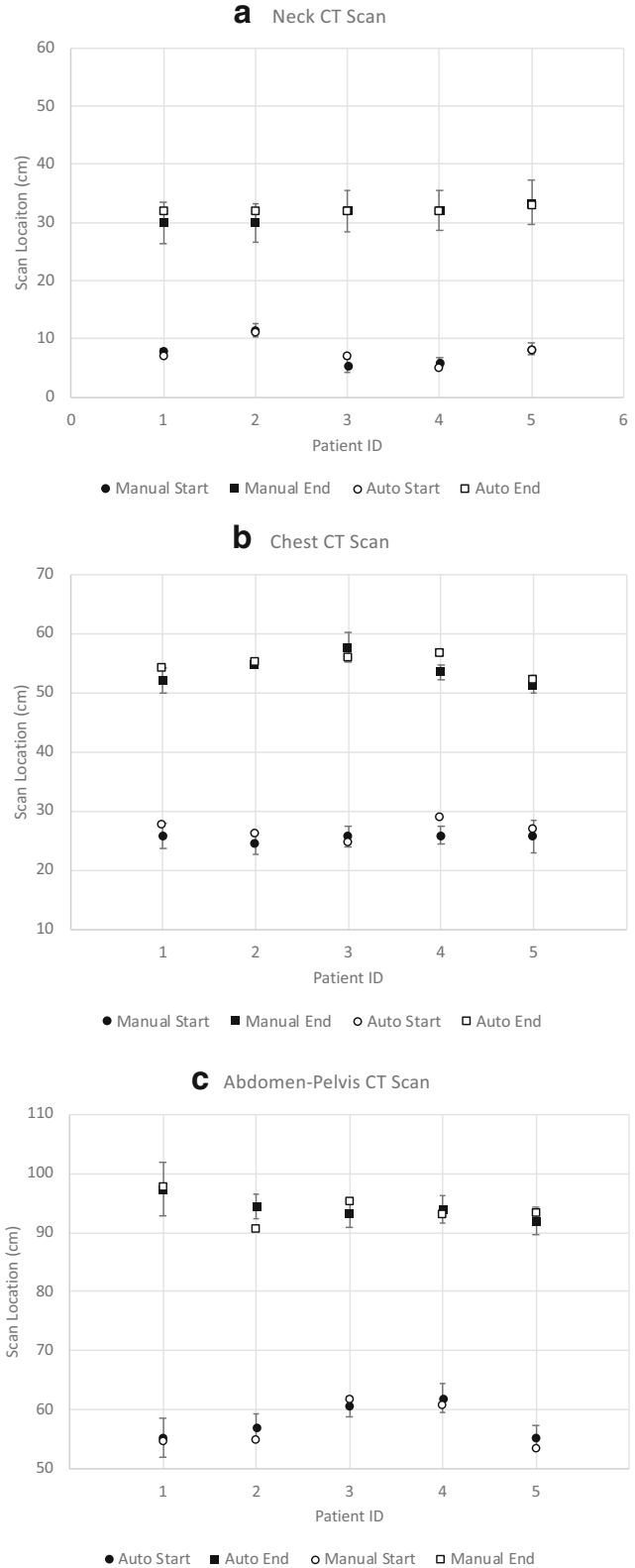

Fig. 3 Comparison of the manual (average and standard deviation across the seven radiologists) and automatic mapping for **a** neck, **b** chest, and **c** AP scans of the five patients

seven radiologists for manual mapping. Figure 2 b, c shows the scan start and end locations for patient 1 manually mapped by radiologists and automatically mapped by the algorithm, respectively. The numbers on the top in each phantom diagram represent the scan start location z cm from the top of the head in the phantom. The numbers on the bottom represent the scan end location. The visual comparison showed excellent agreement between manual and automatic mapping locations for neck, chest, and abdomen-pelvis CTs.

Figure 3 shows the comparison of the manual and automatic mapping for (a) neck, (b) chest, and (c) AP scans of the five patients. Mean and standard deviation for the scan start (solid circle) and end (solid square) locations from the seven radiologists are depicted. For fair comparison of standard deviation, the range of Y axis of each figure is set to 60 cm. The scan location (cm) again stands for the distance from the top of the head in the phantom: smaller numbers represent scan start locations. The variation among the seven radiologists was relatively large for the scan end locations of the neck and AP scans, of which average standard deviations across the five patients were 3.54 and 2.70 cm, respectively. The scan start location of the neck scan shows the smallest variation with the standard deviation of 0.91 cm. Average standard deviations for the scan start and end locations of the chest scans were 1.94 and 1.61 cm, respectively.

Table 1 shows the difference of scan locations between manual (averaged over the seven radiologists' data) and automatic mapping methods for neck, chest, and AP scans. The difference in mapping locations averaged over the start and end in the five patients was less than 1 cm for all neck, chest, and AP scans: 0.9, 0.7, and 0.9 cm for neck, chest, and AP scans, respectively. Five cases out of ten in the neck scans show zero difference between the average manual and automatic mappings. Only one case out of ten shows zero difference in the chest and AP scans. The biggest difference was shown for the scan end location in AP scan of patient 2, where the difference was up to 4 cm. Both scan start and end locations for patient 4 in chest scans also showed relatively large difference, 3 cm.

Comparison of Organ Dose

Organ doses per unit $CTDI_{vol}$ (Gy/Gy) for the average manual mapping locations and the automatic mapping locations were calculated using NCICT. The dose differences (%), (auto − manual)/manual × 100, between the two methods are tabulated in Table 1 for major organs included in the scan coverage in neck, chest, and AP scans. Average of absolute dose differences was 2.3, 2.7, and 4.0% for neck, chest, and AP scans, respectively.

Table 1 Difference in scan location (cm) between manual and automatic mappings and organ dose for neck, chest, and abdomen-pelvis (AP) CT scans. The organs partially included in or close to the scan range are italicized

Scan type	Patient ID	Difference in scan location (cm)		Organ dose difference (%)				
		Start	End	*Brain*	Pituitary gland	Lens	Salivary glands	*Thyroid*
Neck	1	1	2	16	3	1	1	15
	2	0	2	1	0	0	1	15
	3	2	0	− 18	− 4	− 1	0	0
	4	1	0	9	2	0	0	0
	5	0	0	0	0	0	0	0
				Thyroid	*Esophagus*	Lungs	Breast	Heart
Chest	1	2	2	− 14	− 8	1	1	2
	2	2	0	− 5	− 9	− 1	0	0
	3	1	2	3	5	0	− 1	− 1
	4	3	3	− 29	− 13	1	2	3
	5	1	1	− 5	− 4	1	1	2
				Kidney	Small intestine	*Colon*	Urinary bladder	*Prostate*
AP	1	1	0	0	0	0	0	1
	2	2	4	17	3	7	− 3	− 11
	3	1	2	− 22	− 4	− 13	2	6
	4	1	1	28	4	15	− 1	− 3
	5	2	1	4	1	2	1	4

Discussion

In epidemiologic studies or CT clinical research, organ-specific doses are often sought for risk analysis. Although several CT dose calculation tools based on computational human phantoms are currently available to estimate organ doses for CT patients, it is still challenging to accurately map patient-specific scan locations on the phantoms. The aim of the current study was to develop an algorithm to automatically conduct CT-to-phantom mapping.

The variation among the seven radiologists was relatively large for the scan end locations of the neck and AP scans, of which average standard deviations across the five patients were 3.54 and 2.70 cm, respectively. From Fig. 2, it was found that there is no clear anatomical landmark around the scan end location of the neck scan for radiologists to consistently map the location on the phantom. The scan start location of the neck scan shows the smallest variation with the standard deviation of 0.91 cm. Average standard deviations for the scan start and end locations of the chest scans were 1.94 and 1.61 cm, respectively.

The organs located close to the scan boundary or partially included into the scan coverage were underlined. For example, in the neck scans, the brain was partially included in the neck scan coverage and the thyroid is close to the neck scan boundary as shown in Fig. 2. Those underlined organs consistently show relatively larger dose difference between manual and automatic mappings. The thyroid dose in chest scan of patient 4 shows organ dose difference up to 29%. The kidneys in AP scans of patient 4 also show the dose difference of 28%. Those organs partially included or close to the scan boundary may be very sensitive to the scan locations, which are also reported by other studies [10, 18, 27]. The small difference in scan locations can result in significant dose differences: scan start location for AP scans differ only by 1 cm but the kidney doses were different by 28%. The organs completely included in the scan coverage (organs other than those underlined) show excellent agreement with the dose difference less than 5%. The lens and salivary glands in neck scans and the lungs in chest scans show the dose difference less than 1%. Even though the scan start and end locations by manual and automatic methods show some difference up to 2–3 cm, those organs fully included in the scan coverage do not show much difference.

The authors acknowledge the following limitations in the current study. First, the mapping algorithm is based on the comparison of skeletal mask not the location of organs and tissues. Although the best mapping was achieved based on the skeletal mask comparison, the location of organs is still different which would make the resulting organ dose different. Potential abnormal shape or location of organs often observed in patient CTs would not be captured in the automatic mapping process and eventually not reflected in organ dose. Second, there are other factors that affect organ dose but were not taken into account in this study such as the height and weight of patients. We solely focused on mapping process

by matching the dimension of patient CT to that of the computational phantom. As a next step, we are working on the automatic selection of body size-dependent phantoms [28] by using different parameters including water-equivalent diameter. Finally, although we did not observe any case in the current study, it is potentially possible for the automatic mapping algorithm to provide mapping errors. In case of the chest scan mapping in patient 1 (Fig. 1), the algorithm seemed to be confused because of the similarity of skeleton mask between the patient's scapulae and the phantom's pelvis.

Conclusion

We developed an automatic algorithm to map CT scan locations from patients on the computational human phantoms to provide with patient-specific organ doses. From comparison with manual mapping by radiologists, we confirm that our algorithm maps CT on phantoms similar to subjective radiologist assessment in terms of locations. Organ doses based on the automatic mapping locations agreed with those from manual mapping within 4%. The algorithm will be useful in cases requiring patient-specific organ dose for a large number of patients such as patient dose monitoring, clinical trials, and epidemiologic studies.

Funding Information This work was funded by the intramural program of the National Institutes of Health, National Cancer Institute, Division of Cancer Epidemiology and Genetics.

Compliance with Ethical Standards

Disclaimer The contents are solely the responsibility of the authors and does not necessarily represent the official views of the National Institutes of Health.

References

1. Miglioretti DL, Johnson E, Williams A, Greenlee RT, Weinmann S, Solberg LI, Feigelson HS, Roblin D, Flynn MJ, Vanneman N, Smith-Bindman R: The use of computed tomography in pediatrics and the associated radiation exposure and estimated cancer risk. JAMA Pediatr 167(8):700–707, 2013
2. Smith-Bindman R, Miglioretti DL, Johnson E, Lee C, Feigelson HS, Flynn M, Greenlee RT, Kruger RL, Hornbrook MC, Roblin D, Solberg LI, Vanneman N, Weinmann S, Williams AE: Use of diagnostic imaging studies and associated radiation exposure for patients enrolled in large integrated health care systems, 1996-2010. J Am Med Assoc 307(22):2400–2409, 2012. https://doi.org/10.1001/jama.2012.5960
3. NCRP: Ionizing radiation exposure of the population of the United States. Bethesda: National Council on Radiation Protection and Measurement, 2009
4. Harvey HB, Pandharipande PV: The federal government's oversight of CT safety: regulatory possibilities. Radiology 262(2): 391–398, 2012. https://doi.org/10.1148/radiol.11111032
5. McCollough C et al.: The measurement, reporting, and management of radiation dose in CT. Rep AAPM Task Group 23:1–34, 2008
6. AAPM: Size-specific dose estimates (SSDE) in pediatric and adult body CT examinations 2011
7. Simon SL, Kleinerman RA, Ron E, Bouville A: Uses of dosimetry in radiation epidemiology. Radiat Res 166(1 Pt 2):125–127, 2006. https://doi.org/10.1667/RR3385.1
8. Samei E, Tian X, Segars WP: Determining organ dose: the holy grail. Pediatr Radiol 44(S3):460–467, 2014. https://doi.org/10.1007/s00247-014-3117-7
9. Ding A et al: VirtualDose: a software for reporting organ doses from CT for adult and pediatric patients, 5601–5625, 2015, https://doi.org/10.1088/0031-9155/60/14/5601.
10. Lee C, Kim KP, Bolch WE, Moroz BE, Folio L: NCICT: a computational solution to estimate organ doses for pediatric and adult patients undergoing CT scans. J Radiol Prot 35(4):891–909, 2015. https://doi.org/10.1088/0952-4746/35/4/891
11. ImPACT, ImPACT CT Patient Dosimetry Calculator, London, UK 2011.
12. Kalender WA, Schmidt B, Zankl M: A PC program for estimating organ dose and effective dose values in computed tomography. Eur Radiol 9(3):555–562, 1999. https://doi.org/10.1007/s003300050709
13. Sahbaee P, Segars WP, Samei E: Patient-based estimation of organ dose for a population of 58 adult patients across 13 protocol categories. Med Phys 41(7):072104, 2014. https://doi.org/10.1118/1.4883778
14. Stamm G, Nagel HD: CT-expo–a novel program for dose evaluation in CT. RoFo 174(12):1570, 2002
15. Cristy M: Mathematical phantoms representing children of various ages for use in estimates of internal dose. Oak Ridge: Oak Ridge National Laboratory, 1980
16. Xu XG: An exponential growth of computational phantom research in radiation protection, imaging, and radiotherapy: a review of the fifty-year history.R233–R302 2014 https://doi.org/10.1088/0031-9155/59/18/R233
17. Lee C, Lee C, Staton RJ, Hintenlang DE, Arreola MM, Williams JL, Bolch WE: Organ and effective doses in pediatric patients undergoing helical multislice computed tomography examination. Med Phys 34(5):1858–1873, 2007
18. Lee C, Kim KP, Long D, Fisher R, Tien C, Simon SL, Bouville A, Bolch WE: Organ doses for reference adult male and female undergoing computed tomography estimated by Monte Carlo simulations. Med Phys 38(3):1196–1206, 2011
19. Dabin J, Mencarelli A, McMillan D, Romanyukha A, Struelens L, Lee C: Validation of calculation algorithms for organ doses in CT by measurements on a 5 year old paediatric phantom. Phys Med Biol 61(11):4168–4182, 2016. https://doi.org/10.1088/0031-9155/61/11/4168
20. Kim KP, Berrington de Gonzalez A, Pearce MS, Salotti JA, Parker L, McHugh K, Craft AW, Lee C: Development of a database of organ doses for paediatric and young adult CT scans in the United Kingdom. Radiat Prot Dosim 150(4):415–426, 2012. https://doi.org/10.1093/rpd/ncr429
21. Pokora R et al.: Computed tomography in Germany. Dtsch Arztebl Int 113:1–9, 2016. https://doi.org/10.3238/arztebl.2016.0
22. Olerud HM et al: Reconstruction of paediatric organ doses from axial CT scans performed in the 1990s – range of doses as input to uncertainty estimates, Eur Radiol, 1–8,2016 https://doi.org/10.1007/s00330-015-4157-6
23. Bahadori A, Miglioretti D, Kruger R, Flynn M, Weinmann S, Smith-Bindman R, Lee C: Calculation of organ doses for a large number of patients undergoing CT examinations. Am J Roentgenol 205(4):827–833, 2015. https://doi.org/10.2214/AJR.14.14135

24. Lee C, Flynn MJ, Judy PF, Cody DD, Bolch WE, Kruger RL: Body size–specific organ and effective doses of chest CT screening examinations of the National Lung Screening Trial. Am J Roentgenol 208(5):1082–1088, 2017. https://doi.org/10.2214/AJR.16.16979
25. G. Kuzmin et al: A novel method to extend a partial-body CT for the reconstruction of dose to organs beyond the scan range, Radiat Res 2018
26. Lee C, Lodwick D, Hurtado J, Pafundi D, Williams JL, Bolch WE: The UF family of reference hybrid phantoms for computational radiation dosimetry. Phys Med Biol 55(2):339–363, 2010
27. Lee C, Kim KP, Long DJ, Bolch WE: Organ doses for reference pediatric and adolescent patients undergoing computed tomography estimated by Monte Carlo simulation. Med Phys 39(4):2129–2146, 2012. https://doi.org/10.1118/1.3693052
28. Geyer AM et al: The UF/NCI family of hybrid computational phantoms representing the current US population of male and female children, adolescents, and adults–application to CT dosimetry. 5225–5242,2014